Pharmaceutical Research, Vol. 24, No. 7, July 2007 (© 2007)
DOI: 10.1007/s11095-007-9258-8

Research Paper

Confocal Microscopy for the Elucidation of Mass Transport Mechanisms Involved in Protein Release from Lipid-based Matrices

Stephanie Koennings,[1] Joerg Tessmar,[1] Torsten Blunk,[1] and Achim Göpferich[1,2]

Received September 25, 2006; accepted January 31, 2007; published online April 25, 2007

Purpose. It was the aim of this study to identify the governing mechanisms during protein release from cylindrical lipid matrices by visualizing mass transport and correlating the data with *in vitro* dissolution testing.
Materials and Methods. Glyceryl trimyristate cylinders of 2 mm diameter, 2.2 mm height and 7 mg weight were manufactured by compression of a protein–lipid powder mixture prepared by a polyethylene glycol (PEG) co-lyophilization technique. BSA was fluorescence-labeled and the distribution visualized and quantified at different stages of the release process by confocal microscopy in parallel to the quantification in the release buffer. The impact of matrix loading and protein molecular weight was assessed with the model proteins lysozyme, BSA, alcohol dehydrogenase and thyroglobulin.
Results. Buffer penetration and protein release occurred simultaneously from the outer regions of the cylinder progressing towards the center. Release from the top and bottom of the matrix was not negligible but much slower than penetration from the side, probably due to an oriented arrangement of lipid flakes during compression. The different quantification strategies were found to yield identical results. At 6% protein loading, buffer penetration was complete after 4 days, while only 60% of the protein was liberated in that time and release continued up to day 63. Protein release kinetics could be described using the power law equation $M_t/M_\infty = kt^n$ with an average time exponent n of 0.45 (±0.04) for loadings varying between 1 and 8%. A percolation threshold at 5% pure protein loading and 3–4% mixed loading (PEG and protein at a 1:1 mass ratio) could be identified. Release rate was found to decrease with increasing molecular weight.
Conclusions. Protein release from lipid-based matrices is a purely diffusion controlled mechanism. Potential protein stabilization approaches should address the time span between complete buffer penetration of the matrix and 100% release of the remaining loading, which would be exposed to an aqueous environment before leaving the matrix.

KEY WORDS: confocal microscopy; controlled release of proteins; diffusion; lipid matrices; molecular weight; release mechanism.

INTRODUCTION

In controlled release science, substantial research efforts are devoted to the evaluation of suitable matrix materials for the delivery of protein drugs (1). Triglycerides have gained growing attention in this context due to their favorable properties: as physiological substances they have shown good biocompatibility tested subcutaneously (2) and in the brain (3); they are easily compactable and display high long-term stability upon incubation without swelling (4), which qualifies them as a good alternative to commonly used polymeric matrix materials. A successful incorporation into microparticles or cylinders and release thereof has been reported for several peptide and protein drugs and model substances, amongst them insulin (5–7), somatostatin (8), interferon α-2a (9), BSA, hyaluronidase (10), lysozyme, brain derived neurotrophic factor (3) and interleukin-18 (IL-18) (11).

Although stability risks related to the incorporation into polymers, such as the development of an acidic microclimate during incubation (12–14) and the formation of detrimental polymer degradation products (15) can be circumvented by the use of triglyceride matrices, in parallel studies, we have encountered problems during release testing, manifesting in a progressive activity loss (11) or the occurrence of aggregates (3). These effects were more pronounced at higher incubation temperatures suggesting an instability mechanism relat-

[1] Department of Pharmaceutical Technology, University of Regensburg, Universitaetsstr. 31, 93040, Regensburg, Germany.
[2] To whom correspondence should be addressed. (e-mail: achim.goepferich@chemie.uni-regensburg.de)

ABBREVIATIONS: ADH, alcohol dehydrogenase; BCA, biscinchoninic acid; BSA, bovine serum albumin; CLSM, confocal laser scanning microscopy; DCM, dichloromethane; DIPEA, *N*-ethyldiisopropylamine; DMSO, dimethylsulfoxide; FITC, fluorescein isothiocyanate; IL, interleukin; mPEG-NH_2, methoxy-PEG-amine; MWCO, molecular weight cut-off; PEG, polyethylene glycol; TAMRA, carboxy-tetramethylrhodamine; SRH, sulforhodamine 101 hydrate; THF, tetrahydrofurane.

ed to the conditions during *in vitro* dissolution testing. Although a recent mathematical evaluation of data from triglyceride systems has implied a diffusion controlled release mechanism (16), it would be extremely valuable to have a more detailed insight into the mass transport phenomena inside the matrices and obtain quantitative data about the expansion of the aqueous buffer environment, probably being the key towards a better understanding of protein stability. Confocal laser scanning microscopy (CLSM) combines all required features for this task—fluorescently labeled model substances can be visualized within a matrix in a semiquantitative manner (17), allowing the co-localization of several substances in a multitracking mode.

It was therefore the aim of this study to correlate the data obtained from *in vitro* dissolution testing with the information assessed by CLSM to propose a release mechanism and get sensitized for potential stability hazards for proteins incorporated into the matrices. To this end, fluorescent tags were attached to the model substances: BSA was labeled with fluorescein isothiocyanate (FITC) and excipient PEG with carboxytetramethylrhodamine succinimidyl ester (TAMRA-SE). Sulforhodamine 101 hydrate (SRH) was added to the release buffer and its influx monitored to assess the approximate time scale of buffer penetration. To complete the information on the possible release mechanism obtained by this mass transport study, the influence of different loadings and molecular weight was investigated with the model proteins lysozyme (M_w 14 kDa), bovine serum albumin (BSA, M_w 66 kDa), alcohol dehydrogenase (ADH, M_w 150 kDa) and thyroglobulin (M_w 690 kDa). Protein was loaded onto lipid matrix material by a PEG co-lyophilization technique, previously reported by our group for the processing of IL-18 (11).

MATERIALS AND METHODS

Materials

Chicken egg lysozyme (Grade I, M_w 14,000 Da), bovine serum albumin (BSA, Cohn fraction V, M_w 66,000 Da), Bakers yeast alcohol dehydrogenase (ADH, M_w 150 kDa), bovine thyroid thyroglobulin (M_w 690 kDa), bicinchoninic acid disodium salt (BCA), sulforhodamine 101 hydrate (SRH, M_w 607 Da) and Sephadex G10 were purchased from Sigma-Aldrich Chemical Company (Steinheim, Germany). Fluorescein isothiocyanate (Isomer I) and all SDS-PAGE reagents were obtained from Serva (Heidelberg, Germany). Molecular Probes (Leiden, Netherlands) supplied 6-carboxytetramethylrhodamine, succinimidyl ester (6-TAMRA-SE, M_w 528 Da) and Fluka (Buchs, Switzerland) polyethylene glycol (PEG, M_w6,000 Da), dichloromethane (DCM), methanol, tetrahydrofurane (THF), Coomassie® Brilliant Blue G-250, N-ethyldiisopropylamine (DIPEA) and dimethylsulfoxide (DMSO). Methoxy-poly(ethylene glycol)-amine (mPEG-NH_2, M_w 5,000 Da) was from Squarix (Marl, Germany). Copper-(II)-sulfate pentahydrate and sodium azide were purchased from Merck (Darmstadt, Germany). GE Healthcare (Munich, Germany) supplied a HiPrep™ 26/10 desalting column and Carl Roth (Karlsruhe, Germany) Spectra/Por® Biotech membrane (MWCO 3,500 Da). Tissue Tek® was obtained from Sakura Finetek Europe (Zoeterwoude, Netherlands). Witepsol® H37 and glyceryl trimyristate (Dynasan®114) were a gift from Sasol (Witten, Germany).

Fluorescence Labeling of Model Substances

Labeling of PEG

150 mg mPEG-NH_2 and 1 mg 6-TAMRA-SE were dissolved in 10 ml of dichloromethane. DIPEA was added at a molar concentration equal to 6-TAMRA-SE. The solution was stirred under exclusion of light at room temperature for 20 h before the solvent was evaporated under vacuum. Then, 2.5 ml double-distilled water were added to dissolve the product and the mixture was separated on a Sephadex G10 column (50 ml, 2.5×10 cm). Fractions of 0.5 ml were collected and analyzed by thin-layer chromatography for TAMRA-mPEG content and purity (eluent chloroform/ methanol 3:1 (v/v), TLC aluminium sheets silica gel 60 F_{254}, Merck, Darmstadt, Germany). Solutions containing labeled TAMRA-mPEG were freeze-dried and stored at −20°C until further use.

Labeling of BSA

Five milligrams of FITC were dissolved in 0.4 ml DMSO and slowly added to 50 mg BSA in 5 ml 0.1 M disodium carbonate buffer pH 9.0. The mixture was gently stirred under exclusion of light at room temperature for 2 h. Low molecular weight compounds were removed by passage over a HiPrep™ 26/10 desalting column. Fractions containing labeled protein were freeze-dried and stored at −20°C until further use. SDS-PAGE analysis was performed to compare the integrity of labeled to native BSA.

Preparation of Protein-loaded Lipid Matrices

Protein-loaded lipid matrices were obtained by co-lyophilizing a solution of protein in the presence of PEG 6,000 as described recently (11). Briefly, equal amounts of protein and PEG were dissolved in double-distilled water and freeze-dried at 6°C and 0.12 mbar for 30 h in a benchtop freeze-dryer (Beta 2-16 with LMC-2 system control, Christ, Osterode, Germany). The PEG fraction of the lyophilisate was dissolved after removal of vacuum by subsequent addition of THF resulting in a suspension of solid protein particles in organic solvent. To test for the influence of PEG in the formulation, different strategies were pursued. Table I gives an overview of the formulations investigated in this study. PEG was either left in solution and glyceryl trimyristate added at this stage or PEG was removed before the addition of triglyceride. This could be achieved by repeatedly centrifuging the solid protein particles down (12,000 rpm, 10 min, Eppendorf centrifuge 5415R, Eppendorf, Wesseling-Berzdorf, Germany), removing the PEG-containing supernatant and adding fresh THF. After dissolving triglyceride by shortly applying ultrasound (5 s, 5 W), the dispersion was frozen in liquid nitrogen and the organic solvent was removed under a vacuum of 6×10^{-3} mbar for 20 h (Two Stage High Vacuum Pump E2M5, Edwards, Crawley, UK). The resulting dry powder was ground in an agate mortar and compressed in a custom-designed compression tool made of hardened steel

Table I. Composition of Formulations Investigated in this Study

Protein (mg)	PEG 6,000 (mg)	Water (ml)	Triglyceride (mg)	THF (ml)	Total Hydrophilic Loading (%)	Protein Loading (%)
3	3	1	595	2	1	0.5
3	3	1	295	1.5	2	1
5	5	1	325	1.5	3	1.5
5	5	1	240	1.5	4	2
8	8	2	305	1.5	5	2.5
10	10	2	315	1.5	6	3
10	10	2	230	1.5	8	4
3	–	1	295	1.5	1	1
5	–	1	245	1.5	2	2
5	–	1	160	1.5	3	3
8	–	2	190	1.5	4	4
8	–	2	150	1.5	5	5
10	–	2	155	1.5	6	6
15	–	2	175	1.5	8	8
30*	15*/15	5	940	6	6	3
30*	–	5	470	6	6	6

Where (–) is marked in the PEG column, the excipient was initially contained as equal amount to protein and removed after co-lyophilization. (*) stands for fluorescently labeled compounds. Lysozyme served as a model protein in the experiments with different hydrophilic loadings, whereas BSA, ADH and thyroglobulin were incorporated at 6% loading. FITC-BSA was employed for the experiments listed in the bottom two rows. The total hydrophilic loading is the sum of the PEG and the protein content.

(4) to form cylindrical matrices of 2 mm diameter, 2.2 mm height and 7 mg weight. A compression force of 250 N was maintained for 10 s using a Perkin-Elmer hydraulic press (Perkin-Elmer, Ueberlingen, Germany). Matrices were weighed on an analytical balance to determine their exact weight prior to the following release studies.

Release Studies

Quantification of Protein Release

Matrices were incubated in 1.5 ml phosphate buffer pH 7.4 supplemented with 0.01% sodium azide at 37°C. In regular time intervals, buffer was exchanged completely and analyzed for protein content using a micro BCA assay as described by Smith *et al.* (18). Briefly, 100 µl sample and 100 µl bicinchoninic acid disodium salt (BCA) working solution were mixed in a 96-well plate, covered and incubated at 60°C for 1 h. Absorbance was read at 562 nm on a 96-well plate reader (CS-9301 PC, Shimadzu, Duisburg, Germany) after cooling to room temperature. Calibration curves were prepared for each protein separately and corrected for blank readings.

When fluorescent model substances were contained within the matrix, at each sampling time, one set of matrices ($n = 6$) was removed from the incubator and frozen at −20°C. Except for cylinders from buffer penetration studies, matrices were freeze-dried prior to further processing.

Quantitative Determination of PEG

The PEG quantity in the release buffer was assayed by adopting a method described in (19). In brief, a 31% (w/v) solution was prepared from ammonium sulfate dissolved in 0.5 M sodium acetate buffer pH 5 and fluorescein disodium salt hydrate was added to a final concentration of 77 µM. Three hundred microliters of this solution were added to 40 µl sample and

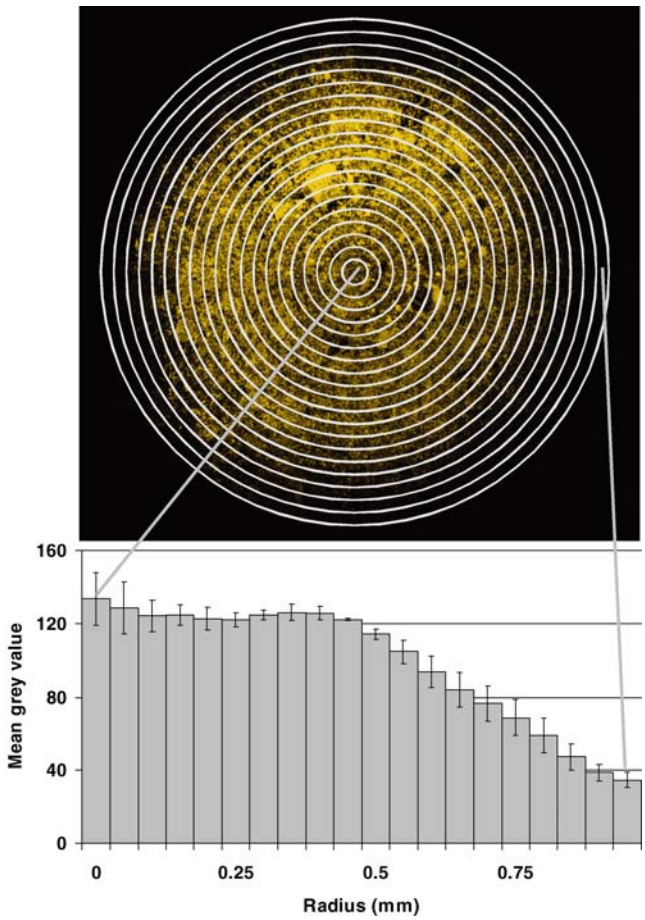

Fig. 1. Schematic illustration of confocal image analysis. *Bars* display mean grey value assessed in concentrical rings superposed as depicted above. *Error bars* represent standard deviation from evaluation of three different cylinders (*cross section*) imaged after identical incubation periods. (Example image was taken after 2 days of incubation, matrix loaded with 6% FITC-BSA).

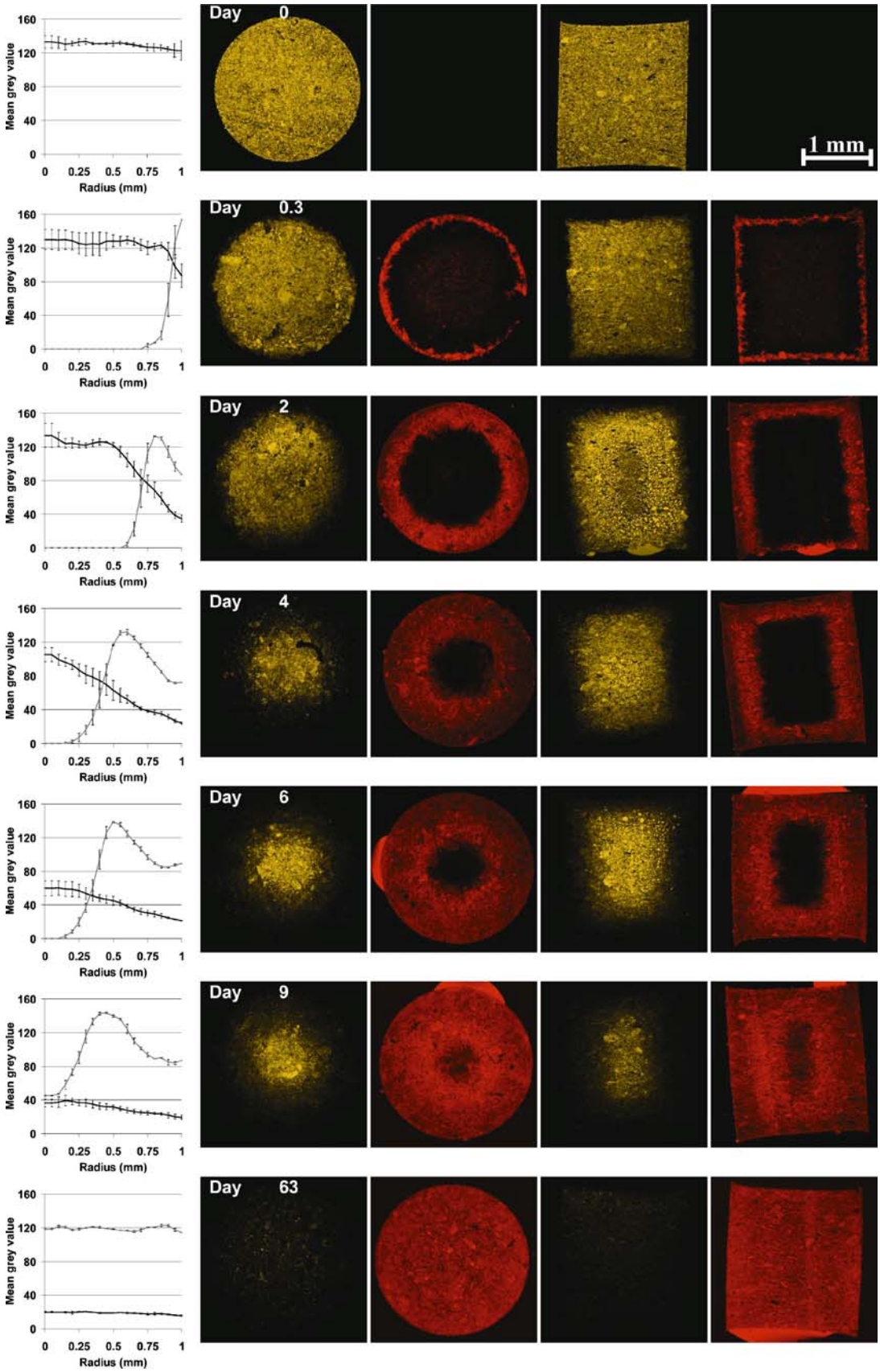

Fig. 2. Changes in fluorescence profiles of cylinder cross sections. Results from image analysis are shown in the first column (*black line*: FITC-BSA, *grey line*: buffer with SRH). Images depict FITC-BSA fluorescence (*left*) together with the corresponding SRH penetration status (*right*) in pairs. The first two images were taken of a transversal cross section, the last two from a longitudinal cut. Samples were taken after 0, 0.3, 2, 4, 6, 9 and 63 days of incubation (*from top to bottom*) of matrices loaded with 6% FITC-BSA.

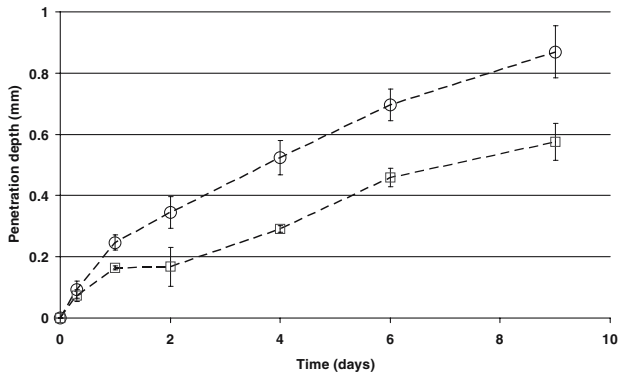

Fig. 3. Comparison of radial (*open circle*) and axial (*open square*) penetration depth of phosphate buffer pH 7.4 containing 0.1 mg/ml sulforhodamin 101 hydrate into glyceryl trimyristate matrices loaded with 6% FITC-BSA.

allowed to settle in the dark for 30 min at room temperature before absorption was measured at 475 nm using a 96-well plate reader. PEG solutions of known concentrations were assayed to obtain a calibration curve.

Confocal Microscopy

Analysis of Protein Content by Cylinder Cross-sections

For easier handling during cross sectioning and microscopic observation, lipid matrices were embedded horizontally ($n = 3$) or vertically ($n = 3$) into a cylinder by melt casting Witepsol® H37 into a ring of 1 cm inner diameter and 1 cm height placed in a flat bottom plastic mold. After solidification in the dark for 2 h, the cylinder was fixed on a sample holder by freezing with Tissue Tek® and cross sections through the matrix center were obtained by cutting on a Microm HM 550 OMP cryotome (Microm, Walldorf, Germany). To protect the cutting area from moisture, Tissue Tek® was removed in the frozen state and cylinders were placed immediately into a desiccator.

Confocal Images

Cross sections were visualized using a Zeiss Axiovert 200M confocal microscope coupled to a Zeiss LSM 510 scanning device (Carl Zeiss Co. Ltd., Germany). The inverted microscope was equipped with a Plan–Neofluar 5×/ 0.15 objective. FITC-BSA was excited at 488 nm and fluorescence was detected using a 505–530 nm band-pass filter whereas SRH was excited at 543 nm and recorded with a 560 nm long-pass filter. Images were taken in the multi-tracking mode. TAMRA-PEG was visualized by excitation at 543 nm and detection above 585 nm using a long-pass filter. Images were processed using the LSM 5 software purchased from Carl Zeiss Co. Ltd., Germany. To ensure that pixel intensities in the images were proportional to drug content, pixel intensity levels were adjusted when the image for time 0 was taken, so that maximum and minimum values were between 0 and 255 grey value in each photomultiplier channel (17). Then, all images determined for quantitative evaluation were taken with the same instrumental settings.

Image Analysis

Cross sections of matrices incubated for different time periods were compared regarding fluorescence profiles for FITC-BSA and SRH. Therefore images from transversal cuts were divided into sections resulting in a grid of 20 concentrical circles with 0.05 mm interspace (see Fig. 1) using LSM 5 software.

For each ring n, the area A_n and the mean grey value as a measure for fluorescence intensity (MGV_n, given by the LSM 5 software as the sum of the grey values of all pixels in the ring divided by the number of pixels) were noted. Total fluorescence I of the cylinder cross section was determined applying Eq. 1 taking into account ring area. For each time point, the transversal cuts from three individual matrices were analyzed.

$$I = \sum_{n=1}^{20} A_n \times MGV_n \tag{1}$$

Investigation of Buffer Penetration Velocity

In parallel to release studies, buffer penetration into the cylinders was monitored on a separate set of matrices by adding 0.1 mg/ml sulforhodamine 101 hydrate to phosphate buffer pH 7.4 that served as release medium. The buffer was exchanged completely at the same time points as for the release study and cylinders were frozen at −20°C before analyzed as described above.

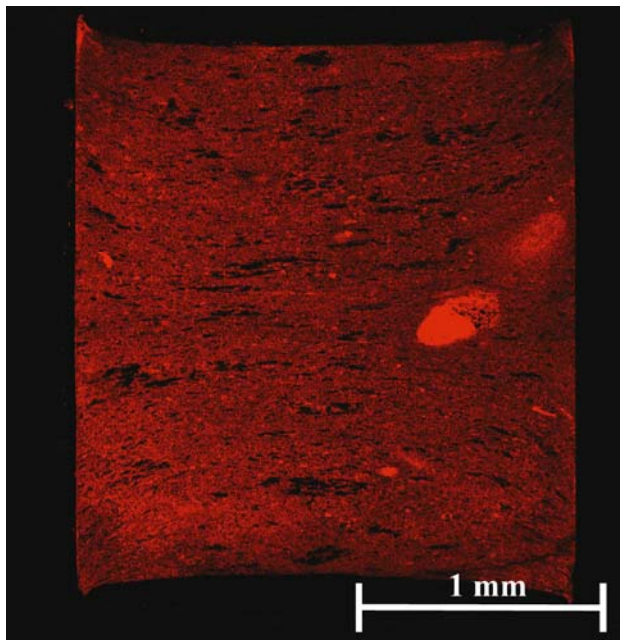

Fig. 4. Longitudinal cross section through a glyceryl trimyristate cylinder after complete release of its protein loading (6% FITC-BSA) and 100% penetration of release buffer with 0.1 mg/ml SRH.

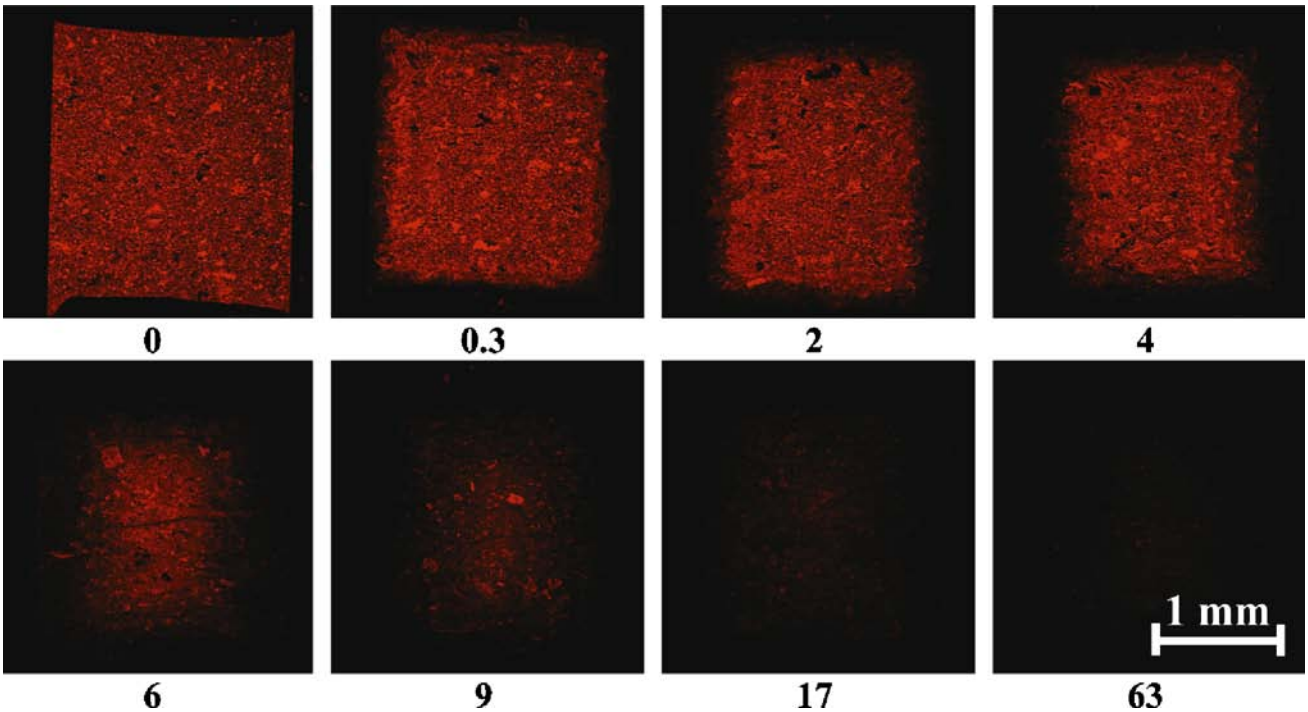

Fig. 5. Changes of TAMRA-PEG fluorescence profiles in longitudinal cylinder cross sections of matrices loaded with 3% protein and 3% PEG (equal amounts of TAMRA-PEG and PEG 6,000). Samples were taken after incubation for the number of days indicated underneath.

Buffer Penetration Depth

In addition to image analysis as described above, for SRH penetration studies, longitudinal cuts ($n = 3$) were compared regarding penetration depth in the radial or axial direction by measuring the distance of the buffer penetration front from the surface of the matrix at the half height and the half diameter using the LSM 5 software.

Statistical Analysis

All measurements were made in triplicate and expressed as means ± standard deviation (SD).

RESULTS

Distribution of Fluorescently Labeled Protein and Buffer

In Fig. 2, the progress of protein release and dye penetration as determined by confocal microscopy can be followed in parallel. While buffer started to penetrate the matrices from the surface progressing towards the center (radius = 0 mm) of the cylinder, the protein in the matrix was depleted simultaneously. In the end, the matrix was void of protein and completely penetrated by buffer. To the left of each set of images, a quantitative evaluation of the situation within the cross section can be found. Before day 4, the protein content within the matrix seemed to be only affected in the outer regions with the loading in the center corresponding to the initial value. A linear slope could be detected across the protein diffusion front. From day 4 on, protein was also depleted from the center of the matrix,

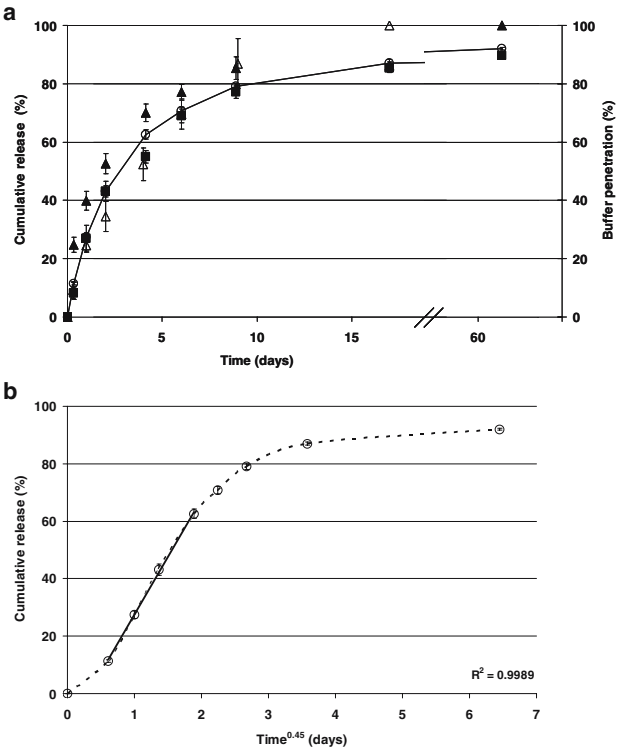

Fig. 6. (**a**) *In vitro* release of FITC-BSA from glyceryl trimyristate matrices loaded with 6% protein (*open cirlce*) and correlation with release quantified by confocal image analysis of non-released FITC-BSA (*closed square*). Comparison to quantification of penetrated buffer containing SRH by confocal image analysis (*closed triangle*) and radial penetration depth measurements (*open triangle*). (**b**) Cumulative amount released plotted versus time$^{0.45}$. The *black line* corresponds to the linear approximation with $R^2 = 0.9989$.

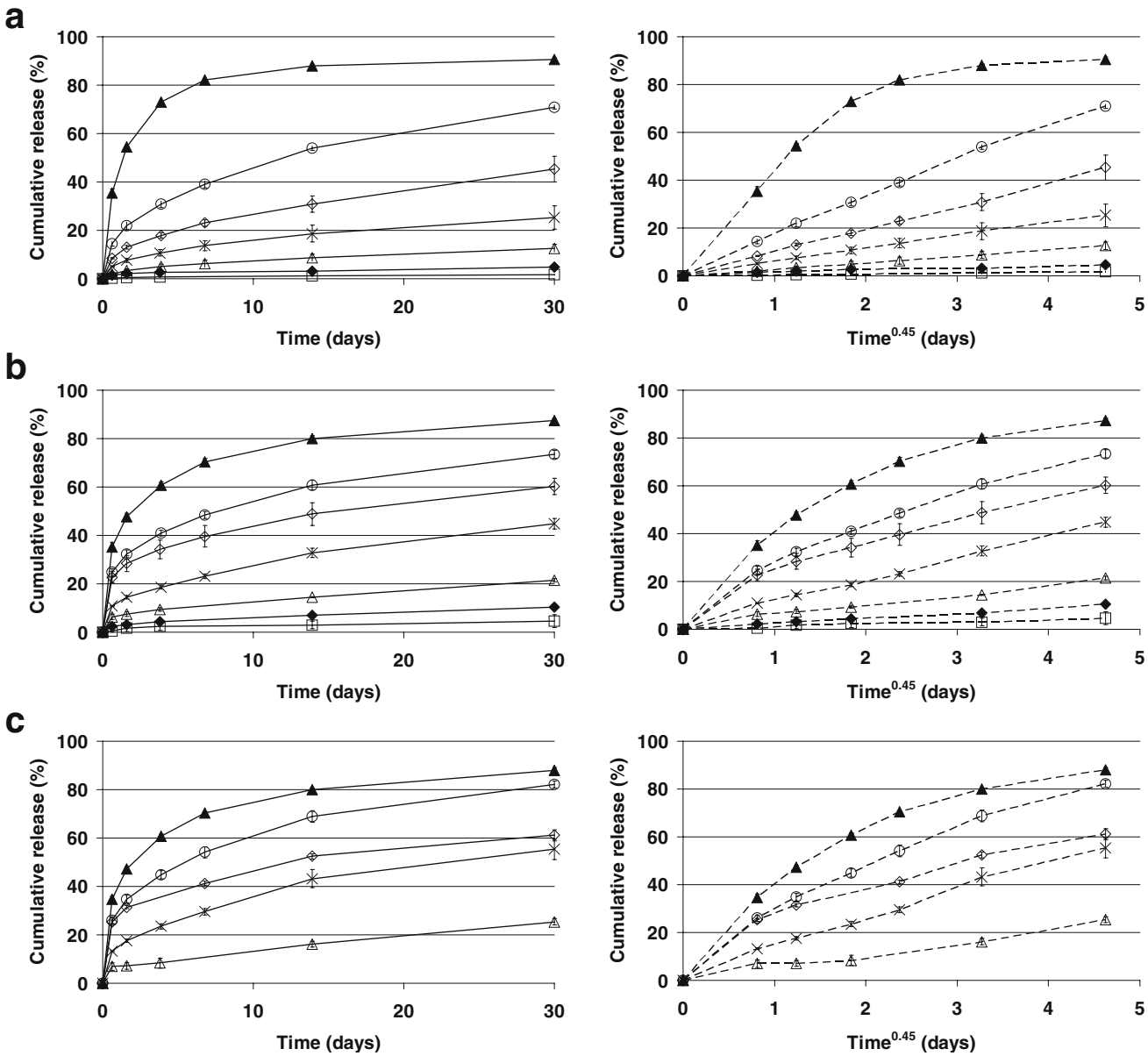

Fig. 7. (**a**) *In vitro* release of lysozyme from glyceryl trimyristate matrices (loading consisted exclusively of protein). (**b**), (**c**) Matrices loaded with equal amounts of protein and PEG 6,000: (**b**) protein release, (**c**) PEG release. Total hydrophilic loading was (*open square*) 1%, (*closed diamond*) 2%, (*open triangle*) 3%, (×) 4%, (*open diamond*) 5%, (*open circle*) 6% and (*closed triangle*) 8% according to Table I.

where the content gradually decreased until the end of release. Although the main peak of the SRH penetration front had not yet reached the matrix center at that time, it was preceded by a diffusion front, which stretched towards the center of the cylinder from day 6 to 9.

When measuring the dye penetration depth in FITC-BSA loaded matrices, the interesting observation was made, that penetration was more extensive from the radial direction of the cylinder compared to the axial direction (Fig. 3). When the matrix was penetrated completely by buffer (Fig. 4), the black areas, indicative of lipid localization, create an impression of a preferential orientation in horizontal layers within the matrix structure.

Figure 5 depicts results for TAMRA-PEG depletion, which were not evaluated quantitatively. It can be seen that labeled PEG is also distributed finely and homogeneously all over the matrix and changes in fluorescence distribution over time closely resemble the ones found for FITC-BSA.

In Vitro Release of Fluorescently Labeled BSA

The release of FITC-BSA from glyceryl trimyristate matrices was determined both by measuring the amount of protein liberated into the release buffer by micro BCA assay and quantification of the non-released fraction with the help of confocal microscopy. Figure 6a gives an overview of the results with the solid line representing the release profile obtained by protein assay. More than 85% of the matrix loading were released within the first 20 days with only a little increase up to 92% until day 63.

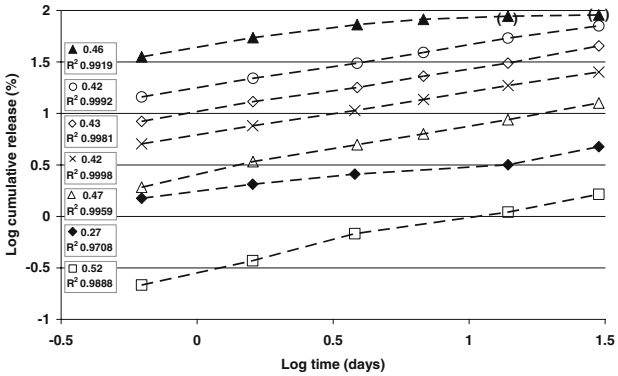

Fig. 8. Logarithm of cumulative release (%) of lysozyme versus logarithm of time for glyceryl trimyristate matrices loaded with (*open square*) 1%, (*closed diamond*) 2%, (*open triangle*) 3%, (×) 4%, (*open diamond*) 5%, (*open circle*) 6% and (*closed triangle*) 8% protein according to Table I. *Boxes on the left hand side* indicate the value for the linear slope of the curve and its correlation coefficient R^2.

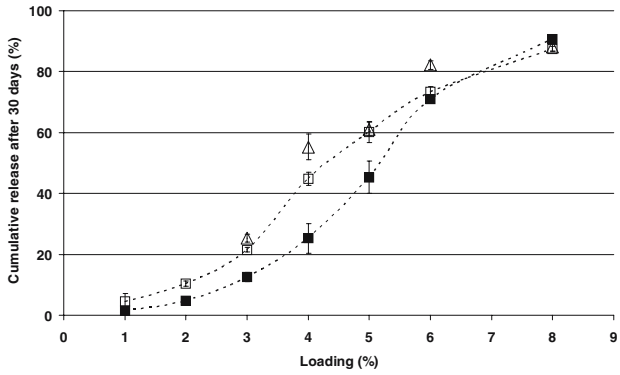

Fig. 9. Amount of protein released after 30 days (%) versus matrix loading for matrices containing only protein (*closed square*) or both protein and PEG 6000 (*open square*) according to Table I. (*Closed triangle*) represents released amounts of PEG 6,000.

The data points obtained by analysis of non-released FITC-BSA by confocal microscopy (black squares) are located close to the release profile in Fig. 6a, indicating that image analysis provides identical information to quantification by protein assay.

In the image, also values from confocal analysis of SRH penetration were included (triangles): Closed triangles represent the amount of dye determined in the cross sections after the different incubation periods related to the amount of dye measured at day 63 in %. While these values were obtained applying Eq. 1 as described under image analysis, open triangles result from radial penetration depth measurements on longitudinal cross sections and are expressed in % of the radius already dyed by SRH. It can be seen, that dye penetration can also be taken as indicative of the amount of protein released, however, it was completed earlier than protein release.

Figure 6b represents a plot of the release data according to the power law equation $M_t/M_\infty = kt^n$ introduced by Ritger and Peppas (20) with the exponent $n = 0.45$ for cylindrical, non-swellable matrices. In the equation, M_t is the cumulative absolute amount of drug released at time t and M_∞ the absolute cumulative amount released at infinitive time, which should be equal to the amount incorporated. k is a constant incorporating structural and geometric characteristics. A good linear correlation ($R^2 = 0.9989$) was obtained for values up to 60% of cumulative release with a lag period occurring during the first 8 h of release.

In Vitro Release of Lysozyme from Matrices with Different Loading

The hydrophilic loading of the lipid matrices varied between 1 and 8%. One set of matrices was loaded exclusively with protein (Fig. 7a), whereas a second set was produced, where the loading was composed of equal amounts of protein and PEG 6,000 (Fig. 7b and c). All experiments showed a strong dependence of the release rate on the loading with faster release occurring at higher loadings.

In the range of 1–5% hydrophilic matrix components, protein release was faster from matrices containing PEG

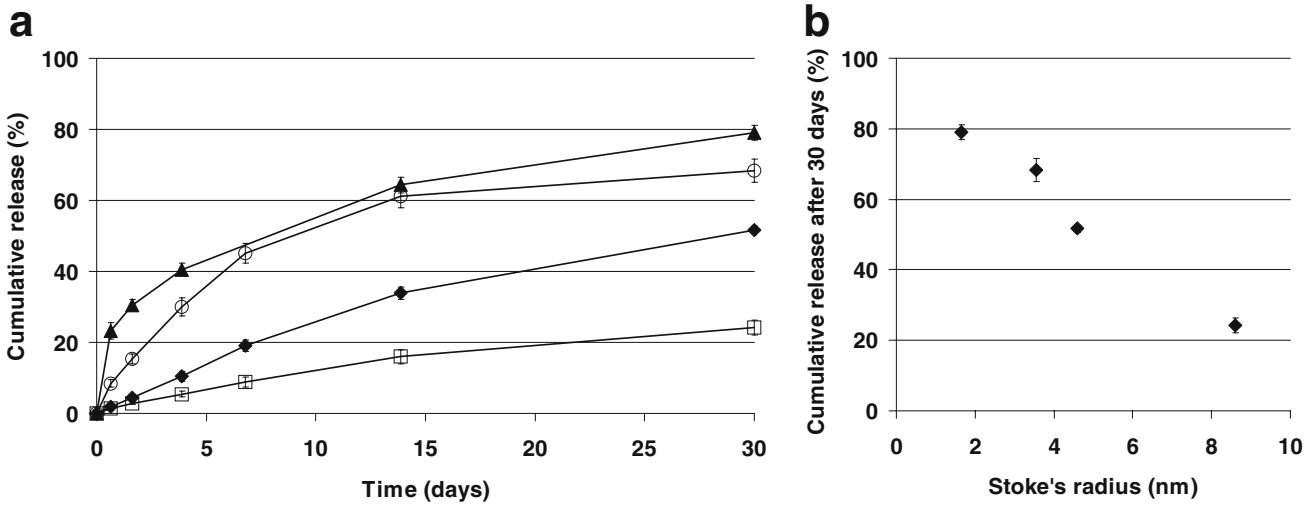

Fig. 10. (**a**) *In vitro* release of (*closed triangle*) lysozyme (14 kDa), (*open circle*) BSA (66 kDa), (*closed diamond*) alcohol dehydrogenase (150 kDa) and (*open square*) thyroglobulin (690 kDa) from matrices loaded with 6% protein. (**b**) Correlation between Stoke's radius of model proteins [(20) and data obtained from the supplier] and cumulative release after 30 days.

(Fig. 7a and b) whereas at 6%, no difference was observed and at 8% matrices without PEG showed an initially faster release. Figure 7c depicts the amount of PEG detected in the release buffer for matrices with 3–8% hydrophilic loading (PEG release for 1 and 2% loading was below the detection limit), which corresponds closely to the amount of lysozyme released, supporting the idea of a parallel release.

A plot of the logarithm of time versus the logarithm of the cumulative lysozyme amount released in % as in Fig. 8 enables the determination of the time exponent n (equal to the slope) for the linear part of the curve according to the power law equation. A linear relationship with good correlation coefficients was observed with all graphs having the same slope but different y-axis intercepts. The mean of the slopes (excluding the value for 2% loading) equaled 0.45 ($\pm$0.04).

To linearize release data, time$^{0.45}$ was then plotted versus cumulative release (%) (Fig. 7, images on the right). In the case of lysozyme, a very good correlation was found; for the profiles of PEG containing matrices, a bend was observed after the first values (corresponding to 15 h) before the profile displayed a linear slope.

Due to the different release rates, the amount of model substance released within 30 days was also found to be a function of the matrix loading. This is illustrated in Fig. 9, with the results shaping into a sigmoidal curve having a inflection point at approximately 5% for matrices loaded with lysozyme alone and between 3 and 4% for matrices with equal content of PEG and lysozyme.

In Vitro Release of Model Proteins with Different Molecular Weight

The release profiles depicted in Fig. 10 show a clear tendency towards a slower release at higher molecular weight of the model compound. When plotting the cumulative amount of protein released after 30 days versus the Stoke's radius of the protein, the impression of a direct relationship between molecule size and release is given.

DISCUSSION

Incorporation of protein into lipid matrix material creates an environment for long-term release (Figs. 6 and 7). Confocal images taken of the matrix cross sections prior to release document a very fine and homogeneous distribution of protein all over the cylinder (Fig. 2, day 0). The porosity of such a matrix, i.e. the space theoretically accessible for release buffer by capillarity and drug dissolution, is composed of void space and drug filled space (22). A compression force of 250 N in this study assured, that air porosity, i.e. void space, was reduced to a minimum, rendering the incorporated amount of drug and excipient the main impact factors for release.

The images in Fig. 2 indicate that protein release and dye penetration are closely related processes. Images were all taken with the same set of parameters in this study with prior adjustment of the instrument settings ensuring that the pixel grey values were proportional to the model substance content allowing for a quantitative analysis. Although the penetration of dye was measured, SRH having low molecular weight (607 Da) and high buffer solubility, it was assumed that this is closely related to the behavior of release buffer itself. The good agreement between the data from methods quantifying FITC-BSA release (BCA assay of released protein and confocal image analysis of non-released protein) with data from analyzing SRH influx into the matrices (Fig. 6a) supports the hypothesis that buffer only penetrates into the matrices, where protein is dissolved and diffuses out. A slight lag between buffer penetration itself and SRH influx might be discussed when interpreting the quantification of FITC-BSA release from day 4 on, where the amount of protein in the center of the matrix started to decrease without the SRH penetration front having fully reached that place (Fig. 2). However, this might also be due to the amount of SRH in the center ranging below the detection limit at the actual instrument settings.

In contrast to SRH penetration depth measurement, SRH profile image analysis of horizontal cross sections indicated a slightly higher buffer content in the matrix than protein released (Fig. 6a). As can be seen in Fig. 2, SRH dye distribution was not homogeneous in the region already penetrated by release buffer with a peak occurring at the buffer penetration front and a decrease in fluorescence towards the matrix surface. Possibly, the height of that peak might be amplified by a faint bleed-through of FITC-fluorescence at high concentrations of freshly dissolved FITC-BSA at the buffer penetration boundary. On day 63, when protein has been completely released, SRH distribution was homogenous all over the cylinder.

Dye penetration depth results in Fig. 6a stemmed from radial measurements of longitudinal cross sections. Interestingly, axial penetration through the cylinders' flat top and bottom surface was less extensive (Fig. 3). As the matrix was manufactured by compression of a powder consisting of anisometric triglycerides flakes, an orientation of the flakes under compression force seems plausible, leading to a higher tortuosity in axial than in radial direction and a better accessibility from the sides of the cylinder. The image of a cylinder completely penetrated by buffer (Fig. 4) supports this hypothesis, as the black areas in the image, where lipid is located, seem to display a preferential orientation of layers in horizontal direction.

Sixty percent of protein was released during the first 4 days (Fig. 6a) of the study, during which the buffer slowly progressed towards the center. The profile of protein distribution within the matrix (Fig. 2, diagrams) showed a linear slope between the buffer penetration front and the cylinder's surface, a typical characteristic of purely diffusion controlled release processes (23,24). When protein started to get depleted also from the center of the cylinder, the protein concentration gradient—being the driving force for its diffusion—gradually decreased, resulting in a slowing of the release rate.

For better visualization, release data was linearized (Fig. 6b) by applying the power law equation. Lipid matrices represent the special case of cylindrical, non-swellable matrices (4) which showed no erosion during the time scale of the experiments (data not shown), where this exponent is postulated to be 0.45 (20) for pure Fickian release behavior. The model allows a prediction up to 60% cumulative release, which in the case of lipid matrices coincides with the slowing of

release due to the decrease in diffusion gradient after complete penetration of the matrices by release buffer. In Fig. 6b, a lag phase can be observed during the first 8 h of release, which is probably due to FITC-BSA being slightly more hydrophobic than the unmodified protein (25), thus showing a reduced capacity to induce matrix wetting by the release buffer and therefore causing a lag in buffer penetration.

The time period between the buffer penetration front reaching the center of the matrix and complete protein release might be critical for protein stability as the remaining loading has to face an aqueous environment while still being inside the matrix. Results from experiments with model proteins of different molecular weight suggest that diffusion is the release rate limiting step (Fig. 10) with an increase in size resulting in a lower diffusion coefficient (26). The difference between the profiles for BSA (Fig. 10) and FITC-BSA (Fig. 6) probably originate in the preparation method where both batches were produced with the same ultrasonication parameters regardless of the batch size. Here, a finer distribution was obtained for the smaller BSA batch.

One approach to limit stability hazards during incubation might be a decrease of buffer penetration speed, e.g. by using a more hydrophobic triglyceride as matrix material. Lower loadings would also represent an alternative, however with the risk of incomplete release.

To test the impact of different loadings, matrices were fabricated with lysozyme as a model substance, which potentially enables the determination of enzymatic activity. Depending on the loading, the fraction of protein having access to the matrix surface via pores created by the release buffer upon its dissolution may vary explaining the shift of the release profiles in Fig. 7. A preliminary evaluation of lysozyme enzymatic activity using the *Micrococcus lysodeikticus* assay (27), however, allowed no conclusions as to protein stability, as lysozyme retained its activity regardless of the loading (data not shown), probably due to its general high stability (28).

In order to assess the time exponent n according to the power law equation at different loadings, release data was plotted as the logarithm of cumulative release versus logarithm of time (Fig. 8), where the slope is representative of the exponent n. The values determined from Fig. 8 by linear correlation showed an excellent fit and were independent of the matrix loading (the profile at 2% loading was considered as outlier due to the inconsistent high release at the beginning). The mean value of 0.45 ($\pm$0.04) for n corresponds to literature data, where n was postulated to equal 0.45 for pure Fickian diffusion in non-swelling matrices as mentioned above (20,23). When plotting the release profiles versus $t^{0.45}$ (Fig. 7), a linearization of the release data could be achieved for all loadings. Release curves of matrices containing hydrophilic PEG showed a slight bend at the beginning, which was maybe due to a better initial wetting. Additionally, PEG—by being able to intersperse the lipid phase upon compression—may increase the amount of protein having access to the surface upon first contact with release buffer. PEG release seems to occur in parallel to lysozyme liberation, only slightly exceeding it up to loadings of 6%, presumably due to the lower molecular weight of the PEG 6,000 resulting in a faster diffusion. In general, the replacement of half the hydrophilic loading by PEG led to an increase in release (Fig. 9) and a higher amount of lysozyme liberated at day 30 for 1–6% loading. A sigmoidal shape of the profile in Fig. 9 was interpreted according to Siegel and Langer (29) as indicative for the hydrophilic loading, above which 100% of the drug can be released as an interconnected network of pores is formed. This critical porosity is reached at the inflection point in the curve, which seems to be at a higher loading for matrices containing only protein (5%) than for PEG-containing matrices (3–4%). The homogeneous distribution of PEG detected by confocal microscopy (Fig. 5) suggests a function as a porogen, preparing a diffusion pathway for the protein. Lower molecular weight and its ability to intermingle with the lipid upon compression might be responsible for slightly lowering that value. Generally, percolation theory as described by Bonny and Leuenberger (30,31) has identified porosities of 20–30% as typical threshold values of inert matrices. However, a dependence of this value on the ratio of drug/matrix particle size was observed shifting it towards lower porosities as the drug particle size decreases (32,33). As the PEG co-lyophilization method leads to a micronization of the protein in the first preparation steps resulting in protein particle sizes below 10 μm (data not shown), the low values obtained in this study are not surprising.

CONCLUSION

A quantitative correlation of *in vitro* dissolution tests and changes of internal matrix composition evaluation by confocal microscopy allowed for the determination of mass transport mechanisms within lipid matrices. Protein release from triglycerides was governed by simultaneous buffer penetration, protein dissolution and its diffusion out of the matrices. Experiments at different loadings and molecular weights all point towards the diffusion being the rate determining step. Potential protein stabilization approaches should address the time span between complete buffer penetration of the matrix and 100% release of the remaining loading, which would be exposed to an aqueous environment before leaving the matrix. However, more sensitive model proteins than lysozyme should be employed to address this topic.

ACKNOWLEDGEMENTS

The authors are grateful for the support of this work by the European Commission (Research and Technological Development Project; BCDDS: Biodegradable Controlled Drug Delivery Systems for the Treatment of Brain Diseases; Contract No.QLK3-CT-2001-02226).

REFERENCES

1. V. R. Sinha and A. Trehan. Biodegradable microspheres for protein delivery. *J. Control Release* **90**(3): 261–280 (2003).
2. C. Guse, S. Koennings, A. Maschke, M. Hacker, C. Becker, S. Schreiner, T. Blunk, T. Spruss, and A. Goepferich. Biocompatibility and erosion behavior of implants made of triglycerides and blends with cholesterol and phospholipids. *Int. J. Pharm.* **314**(2): 153–160 (2006).
3. S. Koennings, A. Sapin, T. Blunk, P. Menei, and A. Göpferich. Towards controlled release of BDNF-Manufacturing strategies for protein-loaded lipid implants and biocompatibility evaluation in the brain. *J. Control Release*, in press (2007).

4. W. Vogelhuber, E. Magni, A. Gazzaniga, and A. Goepferich. Monolithic glyceryl trimyristate matrices for parenteral drug release applications. *Eur. J. Pharm. Biopharm.* **55**(1): 133–138 (2003).
5. B. Appel, A. Maschke, B. Weiser, H. Sarhan, C. Englert, P. Angele, T. Blunk, and A. Gopferich. Lipidic implants for controlled release of bioactive insulin: effects on cartilage engineered *in vitro*. *Int. J. Pharm.* **314**(2): 170–178 (2006).
6. A. Maschke, C. Becker, D. Eyrich, J. Kiermaier, T. Blunk, and A. Gopferich. Development of a spray congealing process for the preparation of insulin-loaded lipid microparticles and characterization thereof. *Eur. J. Pharm. Biopharm.* **65**(2): 175–187 (2007).
7. H. Reithmeier, J. Herrmann, and A. Gopferich. Lipid microparticles as a parenteral controlled release device for peptides. *J. Control Release* **73**(2–3): 339–350 (2001).
8. H. Reithmeier, J. Herrmann, and A. Gopferich. Development and characterization of lipid microparticles as a drug carrier for somatostatin. *Int. J. Pharm.* **218**(1–2): 133–143 (2001).
9. S. Mohl and G. Winter. Continuous release of rh-interferon α-2a from triglyceride matrices. *J. Control Release* **97**(1): 67–78 (2004).
10. W. Vogelhuber, E. Magni, M. Mouro, T. Spruss, C. Guse, A. Gazzaniga, and A. Gopferich. Monolithic triglyceride matrices: a controlled-release system for proteins. *Pharm. Dev. Technol.* **8**(1): 71–79 (2003).
11. S. Koennings, E. Garcion, N. Faisant, J. P. Menei, J. P. Benoit, and A. Goepferich. *in vitro* investigation of lipid implants as a controlled release system for interleukin-18. *Int. J. Pharm.* **314**(2): 145–152 (2006).
12. A. Shenderova, T. G. Burke, and S. P. Schwendeman. Evidence for an acidic microclimate in PLGA microspheres. In *Proceedings of the International Symposium on Controlled Release of Bioactive Materials*, 2001, vol. 25 pp. 265–266.
13. T. Estey, J. Kang, S. P. Schwendeman, and J. F. Carpenter. BSA degradation under acidic conditions: a model for protein instability during release from PLGA delivery systems. *J. Pharm. Sci.* **95**(7): 1626–1639 (2006).
14. G. Zhu and S. P. Schwendeman. Stabilization of proteins encapsulated in cylindrical poly(lactide-co-glycolide) implants: mechanism of stabilization by basic additives. *Pharm. Res.* **17**(3): 351–357 (2000).
15. A. Lucke, J. Kiermaier, and A. Gopferich. Peptide acylation by poly(alpha-hydroxy esters). *Pharm. Res.* **19**(2): 175–181 (2001).
16. C. Guse, S. Koennings, F. Kreye, F. Siepmann, A. Goepferich, and J. Siepmann. Drug release from lipid-based implants: elucidation of the underlying mass transport mechanisms. *Int. J. Pharm.* **314**(2): 137–144 (2006).
17. A. Messaritaki, S. J. Black, C. F. van der Walle, and S. P. Rigby. NMR and confocal microscopy studies of the mechanisms of burst drug release from PLGA microspheres. *J. Control Release* **108**(2–3): 271–281 (2005).
18. P. K. Smith, R. I. Krohn, G. T. Hermanson, A. K. Mallia, F. H. Gartner, M. D. Provenzano, E. K. Fujimoto, N. M. Goeke, B. J. Olson, and D. C. Klenk. Measurement of protein using bicinchoninic acid. *Anal. Biochem.* **150**:76–85 (1985).
19. C. Guermant, J. Brygier, D. Baeyens-Volant, M. Nijs, J. Vincentelli, C. Paul, and Y. Looze. Quantitative determination of polyethylene glycol based upon its salting out and partitioning of a dye into the resulting aqueous two-phase system. *Anal. Biochem.* **230**(2): 254–258 (1995).
20. P. L. Ritger and N. A. Peppas. A simple equation for description of solute release: I. Fickian and non-fickian release from non-swellable devices in the form of slabs, spheres, cylinders or discs. *J. Control. Release.* **5**(1): 23–36 (1987).
21. M. Le Maire, A. Ghazi, J. V. Moeller, and L. P. Aggerbeck. The use of gel chromatography for the determination of sizes and relative molecular masses of proteins. Interpretation of calibration curves in terms of gel-pore-size distribution. *Biochem. J.* **243**(2): 399–404 (1987).
22. F. Carli and L. Simioni. Kinetics of liquid capillary penetration into inert polymer matrixes. *Pharm. Acta Helv.* **53**(11): 320–326 (1978).
23. R. Collins. Mathematical modelling of controlled release from implanted drug-impregnated monoliths. *Pharm. Sci. Technol. Today* **1**(6): 269–276 (1998).
24. P. Colombo, R. Bettini, P. L. Catellani, P. Santi, and N. A. Peppas. Drug volume fraction profile in the gel phase and drug release kinetics in hydroxypropyl methyl cellulose matrixes containing a soluble drug. *Eur. J. Pharm. Biopharm.* **9**(1): 33–40 (1999).
25. S. W. Sun, Y. I. Jeong, S. W. Jung, and S. H. Kim. Characterization of FITC-albumin encapsulated poly(DL-lactide-co-glycolide) microspheres and its release characteristics. *J. Microencapsul.* **20**(4): 479–488 (2003).
26. O. Hosoya, S. Chono, Y. Sako, K. Juni, K. Morimoto, and T. Seki. Determination of diffusion coefficients of peptides and prediction of permeability through a porous membrane. *J. Pharm. Pharmacol.* **56**(129): 1501–1507 (2004).
27. D. Shugar. Measurement of lysozyme activity and the ultraviolet inactivation of lysozyme. *Biochim. Biophys. Acta* **8**:302–309 (1952).
28. P. Jolles and J. Jolles. What's new in lysozyme research? Always a model system, today as yesterday. *Mol. Cell. Biochem.* **63**(2): 165–189 (2001).
29. R. A. Siegel, J. Kost, and R. Langer. Mechanistic studies of macromolecular drug release from macroporous polymers. I. Experiments and preliminary theory concerning completeness of drug release. *J. Control Release* **8**(3): 223–236 (1989).
30. J. D. Bonny and H. Leuenberger. Matrix type controlled release systems: I. Effect of percolation on drug dissolution kinetics. *Pharm. Acta Helv.* **66**(5–6): 160–164 (1991).
31. J. D. Bonny and H. Leuenberger. Matrix type controlled release systems II. Percolation effects in non-swellable matrices. *Pharm. Acta Helv.* **68**(1): 25–33 (1993).
32. I. Caraballo, M. Millán, and A. M. Rabasco. Relationship between drug percolation threshold and particle size in matrix tablets. *Pharm. Res.* **13**(3): 387–390 (1996).
33. M. Millán, I. Caraballo, and A. M. Rabasco. The role of the drug/excipient particle size ratio in the percolation model for tablets. *Pharm. Res.* **15**(2): 216–220 (1998).